THE JOURNAL OF PHYSICAL CHEMISTRY LETTERS
A JOURNAL OF THE AMERICAN CHEMICAL SOCIETY

pubs.acs.org/JPCL

Letter

Non-Newtonian Dynamics in Water-in-Salt Electrolytes

Tsuyoshi Yamaguchi, Andrei Dukhin, Young-Jay Ryu, Dongzhou Zhang, Oleg Borodin, Miguel A. González, Osamu Yamamuro, David L. Price, and Marie-Louise Saboungi*

Cite This: *J. Phys. Chem. Lett.* 2024, 15, 76–80

Read Online

ACCESS | Metrics & More | Article Recommendations | Supporting Information

ABSTRACT: Water-in-salt electrolytes have attracted considerable interest in the past decade for advanced lithium-ion batteries, possessing important advantages over the non-aqueous electrolytes currently in use. A battery with a LiTFSI–water electrolyte was demonstrated in which an operating window of 3 V is made possible by a solid–electrolyte interface. Viscosity is an important property for such electrolytes, because high viscosity is normally associated with low ionic conductivity. Here, we investigate shear and longitudinal viscosities using shear stress and compressional longitudinal stress measurements as functions of frequency and concentration. We find that both viscosities are frequency-dependent and exhibit almost identical frequency and concentration dependences in the high-concentration region. A comparison to quasielastic neutron scattering experiments suggests that both are governed by structural relaxation of the $TFSI^-$ network. Thus, LiFTSI–water electrolytes appear to be an unusual case of a non-Newtonian fluid, where shear and longitudinal viscosities are determined by the same relaxation mechanism.

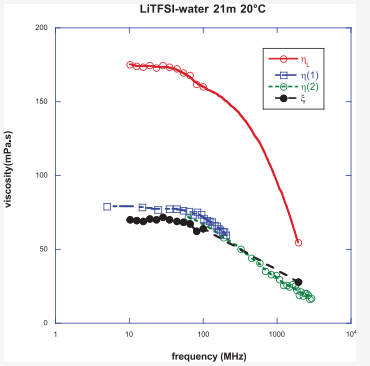

Suo et al.[1] reported several favorable properties of LiTFSI-based water-in-salt electrolytes, including a high electrochemical stability window, good thermal stability, and high lithium ion conductivity. In subsequent work, Borodin et al.[2] combined molecular dynamics (MD) numerical simulations with pulsed-field gradient nuclear magnetic resonance (PFG-NMR) diffusion to establish that nanoscale heterogeneity influences the structural and dynamic properties in this class of aqueous electrolytes and that the high Li^+ contribution to conductivity could be attributed to high salt dissociation and fast $Li^+(H_2O)_4$ diffusion through the water-rich nanodomain, while the negatively charged ionic framework relaxed much slower. Detailed diffraction,[3,4] quasielastic neutron scattering (QENS),[5,6] and Fourier transform infrared spectroscopy (FTIR)[6] investigations have, despite some minor quantitative differences with the MD predictions, largely confirmed this scenario. A network consisting of free species and finite clusters derived from a thermodynamic model of reversible ionic aggregation and gelation[7,8] shows similar features.

Shear viscosity is an important property for electrolytes, because high viscosity is normally associated with low ionic conductivity, and in fact, inverse viscosity and conductivity exhibit a nearly linear relation as a function of the concentration in LiTFSI–water electrolytes.[2] The challenge of decoupling electrical and mechanical relaxation in polymer electrolytes was identified 30 years ago by Angell et al.[9] and in this system addressed by the high salt dissociation and nanoscale heterogeneity already referenced. However, in non-Newtonian fluids, the shear viscosity is dependent upon the shear rate or shear rate history and cannot be considered a fluid property. In this paper, we examine whether such behavior is encountered in the LiTFSI–water system and determine the frequency and concentration dependence of both the shear viscosity and longitudinal viscosity. We measure the longitudinal viscosity in addition to the shear viscosity because it contains contributions of rotational and vibrational degrees of freedom of molecular motion in addition to the translational degree of freedom that controls shear viscosity.

We carried out frequency-dependent shear viscosity measurements using the transverse ultrasound technique reported by Yamaguchi and Matsuoka.[10] Results for LiTFSI–water at 21 m concentration are shown in Figure 1a and compared to those for pure water[8] obtained with the same procedure in Figure 1b.

Two remarkable features are apparent in Figure 1a: the real component of the shear viscosity displays relaxation beginning at about 80 MHz, and this is mirrored by an imaginary component that appears at about the same frequency and peaks at around 500 MHz. The imaginary part of the viscosity describes the elastic response of the liquid, and the inverse of the peak frequency describes the relaxation time of the fluctuation of the stress tensor, which is related to the time scale of the dynamics of microscopic dynamics that governs the viscosity. The behavior shown in Figure 1a signifies that the LiTFSI–water electrolyte is exhibiting non-Newtonian behav-

Received: November 8, 2023
Revised: December 9, 2023
Accepted: December 20, 2023
Published: December 22, 2023

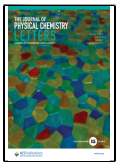

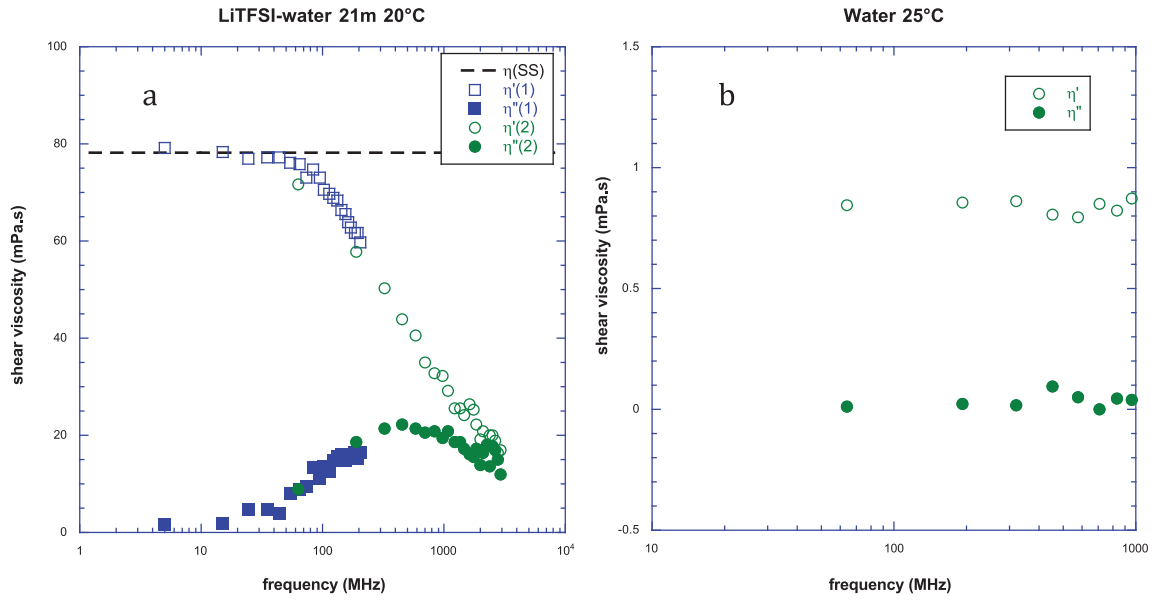

Figure 1. Frequency-dependent shear viscosity in (a) LiTFSI−water at 21 m concentration and 20 °C and (b) pure water at 25 °C.[10] The real (η') and imaginary (η'') components are denoted by open and solid symbols, respectively. The black dashed line in panel a shows the steady-state viscosity; the blue symbols labeled $\eta'(1)$ and $\eta''(1)$ in panel a denote measurements taken with a gold-coated quartz transducer; and the green symbols labeled $\eta'(2)$ and $\eta''(2)$ in panel a and η' and η'' in panel b denote measurements taken with an electrodeless quartz transducer.

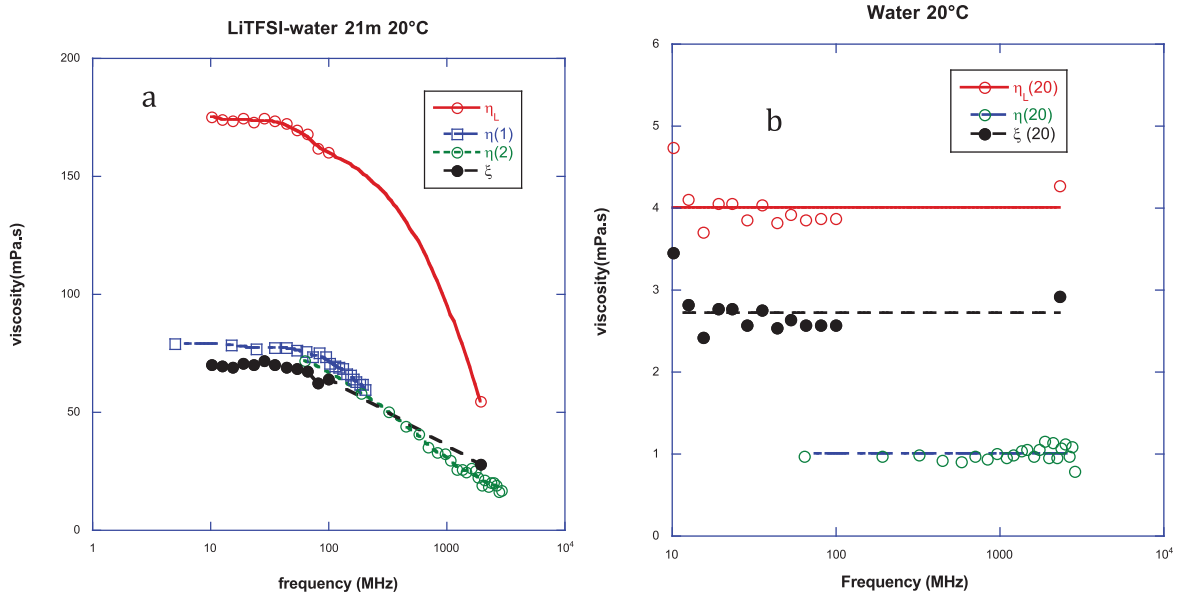

Figure 2. Frequency-dependent shear (η, blue and green symbols), longitudinal (η_L, red symbols), and bulk (ξ, black symbols) viscosities in (a) LiTFSI−water at 21 m concentration and 20 °C and (b) pure water at 20 °C. Notation for the shear viscosity results follows that in Figure 1. The longitudinal viscosity results between 10 and 100 MHz were obtained with acoustic spectroscopy, and that at 1960 MHz was obtained with Brillouin scattering. The results for the shear viscosity of water at 25 °C from ref 10 shown in Figure 1b were multiplied by 1.14 (ratio of the shear viscosity at 20 °C to that at 25 °C from ref 15) to provide equivalent values for 20 °C. The continuous curves in panel a represent guides to the eye, and those in panel b average over the measured frequency ranges.

ior in the frequency range from 80 MHz to 3 GHz. Non-Newtonian behavior of the shear viscosity has also been observed in simulations[11] of a room-temperature ionic liquid [emim][Ntf2]. In contrast to water (Figure 1b) follows Newtonian dynamics in the same frequency region, although there is evidence from both simulation and experiment of non-Newtonian behavior at terahertz frequencies.[12]

We carried out the longitudinal viscosity measurements using the acoustic spectroscopy technique reported by Dukhin and Goetz[13] over the frequency range of 1−100 MHz. This method employs a pulse technique for measuring attenuation (α_L) and sound speed (v_L) of compressional longitudinal waves in a liquid sample. The longitudinal viscosity η_L is then calculated using following equation:[13]

$$\eta_L = \frac{2\alpha_L \rho {v_L}^3}{\omega^2} \quad (1)$$

where ρ and ω are the density and circular frequency, respectively. All of these parameters are either measured or known.

https://doi.org/10.1021/acs.jpclett.3c03145
J. Phys. Chem. Lett. 2024, 15, 76−80

To extract the contribution of rotational and vibrational degrees of freedom, we followed the notion of "bulk viscosity (ξ)" introduced by Sir Horace Lamb in 1879.[14] It can be calculated from the longitudinal viscosity using following equation:

$$\xi = \eta_L - 4/3\eta \quad (2)$$

where η is the shear (or dynamic) viscosity. This equation was derived for Newtonian liquids. Samples that we study here are Newtonian within the frequency range up to almost 100 MHz, because neither shear nor longitudinal viscosity is frequency-dependent within this range. This fact provides us with justification of using eq 2 and the notion of "bulk viscosity" for the samples studied. We extend these calculations even to higher frequency for approximate estimates of other degrees of freedom besides translational.

To obtain a value at higher frequency to combine with the high-frequency shear viscosity value shown in Figure 1a, Brillouin scattering measurements were made with a laser wavelength of 532 nm and a fixed scattering angle of 50°. Results for LiTFSI–water at 21 m concentration are shown in Figure 2a and compared to those for pure water obtained with the same procedure in Figure 2b. The latter are in agreement with the literature.[15]

The frequency dependence of the bulk viscosity in Figure 2a is remarkably similar to that of the shear viscosity and, at this concentration, almost overlays it. The evolution of the two viscosities as the salt concentration is increased as shown in Figure 3 (left vertical scale). Both exhibit a monotonic increase from pure water to the 21 m concentration, show a remarkably similar concentration dependence, and are almost superimposed over the high concentration range of 10–21 m. The bulk/shear ratio (right vertical scale) similarly shows a monotonic decrease from 2.7 in pure water to 0.9 in the 21 m electrolyte.

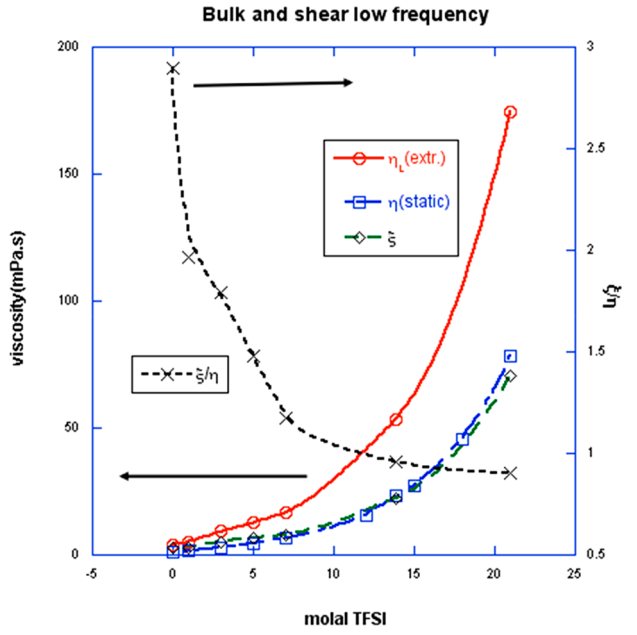

Figure 3. Concentration dependence of the shear (η, blue symbols), longitudinal (η_L, red symbols), and bulk (ξ, black symbols) static viscosities in LiTFSI–water solutions and concentration dependence of the bulk/shear viscosity ratio (black crosses). The values of η_L shown in Figure 2a were extrapolated to zero frequency by fitting the function $(a + b\nu^2)$ to the low-frequency data. The continuous curves represent guides for the eye.

Two immediate questions follow from the results shown in Figures 2 and 3: (1) Why do the two viscosities have similar frequency dependence and, in the high-concentration region, similar concentration dependence? (2) Why does the bulk/shear viscosity ratio decrease with the concentration?

An answer to the first question is suggested by examining the total intermediate scattering function $I_{tot}(Q, t)$ derived from QENS measurements by González et al.,[5] where Q represents the scattering vector and t the evolution time of the system. The stretched exponential (KWW) fits to the experimental $I_{tot}(Q, t)$ values reported there were squared and back-Fourier-transformed to give the function $G(Q, \nu)$, where ν is the temporal frequency. The procedure used is discussed in the Supporting Information. The results for LiTFSI–D_2O 21 m at 27 °C are compared in Figure 4 with frequency-dependent shear viscosity results at 25 °C. The comparison is made with the deuterated solution because, in that case, the scattering is mainly coherent and, thus, reflects collective rather than single-particle excitations. The bulk viscosity values from Figure 2a, adjusted for the temperature change from 20 to 25 °C, are also included in the figure.

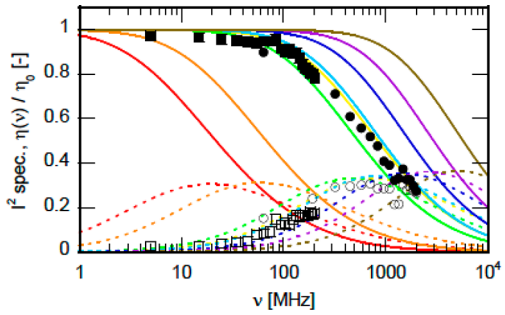

Figure 4. (Continuous curves) Functions $G(Q, \nu)$ derived from intermediate scattering functions $I_{tot}(Q, t)$ fitted to QENS results[5] for LiTFSI–D_2O 21 m at 27 °C. The real and imaginary components are denoted by solid and dotted curves, respectively, and correspond to Q = 0.4, 0.6, 0.8, 1.0, 1.2, 1.4, 1.6, and 1.8 Å^{-1}, reading from left to right. (Squares and circles) Frequency-dependent shear viscosity in LiTFSI–water 21 m, at 25 °C. The real and imaginary components are denoted by open and solid symbols, respectively. (Green triangles) Frequency-dependent bulk viscosity. The data in Figure 2a were multiplied by 0.81 (ratio of the shear viscosity at 25 °C to that at 20 °C) to provide equivalent values for 25 °C.

Both bulk and shear viscosity relaxation are seen to match extremely well with the QENS correlation functions derived from the QENS results from ref 5 for Q values in the range of 1.0–1.2 Å^{-1}, suggesting that structural relaxation in this Q range is an important factor in both viscosity mechanisms. This range of Q is significant because $TFSI^-$–$TFSI^-$ correlations dominate the peak in the weighted average interference function measured in diffraction experiments (Figure S1 of the Supporting Information). The relaxation of this network, much slower than that of the lithium ions and water molecules according to the NMR[2] and QENS[5] measurements, appears to govern both the bulk and shear viscosity in this system.

The second question posed above deals with the different behavior between LiTFSI–water solutions and pure water, in particular the different values of the bulk/shear viscosity ratio. The bulk viscosity of water has been measured by Dukhin and

https://doi.org/10.1021/acs.jpclett.3c03145
J. Phys. Chem. Lett. 2024, 15, 76–80

Goetz[13] and Holmes et al.[15] Dukhin and Goetz present a comparison of the two viscosities for a variety of Newtonian and non-Newtonian fluids, showing that the ratio of the two can have a wide range of values; i.e., the two viscosities are not necessarily correlated with each other or with other physical properties, such as density, dielectric permittivity, and compressibility. Thus, the LiTFSI−water solutions studied here may be an unusual case where the two viscosities are mainly determined by the same structural relaxation mechanism.

Numerical simulations can provide valuable insights into the behavior of the two viscosities. Jaeger et al.[16] have studied the bulk viscosity of water with molecular simulations based on Green−Kubo relations for the fluctuations of the pressure tensor and discussed its relation to the shear viscosity. Such a simulation involves the pressure tensor, and to compute it, one needs to track not only the atomic positions but also the velocities and forces acting in each atom, neither available in the trajectories computed in most simulations, including those reported in refs 1−5. It is hoped that the present work might stimulate numerical studies of the bulk viscosity in water-in-salt electrolytes, such as the system studied here.

Experimental Methods. *Material Preparation*. For steady-state and frequency-dependent shear viscosity measurements, LiTFSI (lithium battery grade, Kishida, Japan) was dissolved in Milli-Q water made by Simplicity UV (Merck, Germany).

Transverse Ultrasound. The density and steady-state shear viscosity were measured by a Stabinger viscometer (SVM-3001, Anton Paar, Austria). For the measurement of frequency-dependent viscosity, we employed two spectrometers that cover from 5 to 205 MHz and from 65 MHz to 3 GHz, respectively. Both spectrometers are based on the quartz crystal microbalance with dissipation (QCM-D) method, in which the changes in the resonance properties of an AT-cut quartz transducer upon the contact with the sample liquid were measured for the determination of the complex shear viscosity at the resonance frequencies. In the first spectrometer, a commercial transducer with gold electrodes (QSX 301, Biolin, Sweden), whose fundamental frequency is 5 MHz, was used, and the resonance properties were measured using a homemade electric bridge and a vector network analyzer (ZVL3/03, Rhode & Schwarz, Germany).[17,18] The second spectrometer uses an order-made electrodeless quartz transducer whose fundamental frequency is 65 MHz. The resonance properties were determined with a vector network analyzer (ZNL3, Rhode & Schwarz, Germany) through the complex reflectance (S_{11}) measurement. The details of the measurement were described elsewhere.[10]

Acoustic Spectroscopy. In this study, acoustic spectrometer DT-100 of Dispersion Technology, Inc. was used. A detailed description of this device is provided in ref 13. The two essential features of the acoustic measurements that make it absolute (requiring no calibration) are pulse signal processing and a variable path for ultrasound pulse propagation. The electronics of this instrument are capable of generating short square electric pulses filled with different frequencies, from 1 to 100 MHz. A piezoelectric transducer (transmitter) converts these pulses to sound pulses of the same frequency. These ultrasound pulses propagate through a liquid sample, interact with the liquid and particles, and consequently attenuate. A second transducer (receiver) converts the received weaker sound pulses back into electric pulses. A comparison of the initial and final electric pulses serves as a measurement of energy loss within the liquid sample.

The distance between the transmitter and receiver varies in steps. In default, it is set to perform 21 steps from 0.3 to 20 mm. This variable gap method makes the application of the Beer−Lambert law possible. According to this absolute law, the ratio of ultrasound intensities measured at different gaps between the transmitter and receiver and expressed in decibels (logarithm on a decimal basis) should be a linear function of the gap. This conclusion is easily verifiable experimentally, and observed linearity confirms the Beer−Lambert law. The slope of each linear regression is the desirable attenuation coefficient at that frequency. This method eliminates calibration because, instead of absolute energy, the acoustic sensor measures the rate of energy loss.

The other important advantage of this method is the low sensitivity to contamination of the transducer surfaces. Concentrated samples could potentially build up deposits on the faces of the two transducers. These deposits of particles would affect absolute acoustic energy but not the rate of its decay during pulse propagation through the sample.

Brillouin Scattering. Brillouin spectroscopy was performed at the GSECARS 13-BM-D beamline at the Advanced Photon Source, Argonne National Laboratory. Brillouin spectra were collected at 20 °C using a Coherent Verdi V2 continuous wave solid-state laser with a wavelength of 532 nm and a power output of 300 mW, in addition to a Hamamatsu detector featuring a typical dark count of 7 counts/s. A Sanderock-type six-pass tandem Fabry−Pérot interferometer was also utilized.[19] Equal angle geometry (θ = 49.4°) was used so that the refractive index of the liquid is not needed. The liquid sample was placed in a sealed quartz glass jar, and the incident laser beam was focused to a 7 μm spot. The Brillouin system was calibrated using the sound speed of deionized water at 20 °C (1481 m/s). The sound speed of the liquid is sensitive to the temperature of the sample. To cross check the potential heating from the Brillouin excitation laser, we did the calibration with three different laser powers, 500, 50, and 3 mW, and all three measurements gave consistent sound speeds of water (1484 ± 5 m/s for 500 mW, 1482 ± 5 m/s for 50 mW, and 1480 ± 5 m/s for 3 mW), indicating that the excitation laser will not heat the transparent sample. The measurements on the LiTFSI−water solutions were carried out with the lowest laser power (3 mW). The Brillouin data were collected using the Win1024 software.[20]

■ ASSOCIATED CONTENT

Supporting Information

The Supporting Information is available free of charge at https://pubs.acs.org/doi/10.1021/acs.jpclett.3c03145.

Neutron-weighted average interference functions for 21 m LiTFSI−H_2O (Figure S1); calculation of the function G(Q, υ) displayed in Figure 4 of the main paper (PDF)

■ AUTHOR INFORMATION

Corresponding Author

Marie-Louise Saboungi − *IMPMC, Sorbonne Université and CNRS, F-75252 Paris, France*; Email: ml.saboungi@gmail.com

https://doi.org/10.1021/acs.jpclett.3c03145
J. Phys. Chem. Lett. 2024, 15, 76−80

Authors

Tsuyoshi Yamaguchi − *Graduate School of Engineering, Nagoya University, Nagoya, Aichi 464-8603, Japan;* orcid.org/0000-0003-4590-8592

Andrei Dukhin − *Dispersion Technology, Incorporated, Bedford Hills, New York 10507, United States*

Young-Jay Ryu − *Center for Advanced Radiation Sources, The University of Chicago, Chicago, Illinois 60637, United States;* orcid.org/0000-0002-1322-0198

Dongzhou Zhang − *Center for Advanced Radiation Sources, The University of Chicago, Chicago, Illinois 60637, United States;* orcid.org/0000-0002-6679-892X

Oleg Borodin − *Energy Storage Branch, Sensor and Electron Devices Directorate, United States Army Research Laboratory, Adelphi, Maryland 20783, United States;* orcid.org/0000-0002-9428-5291

Miguel A. González − *Institut Laue Langevin, 38042 Grenoble, France;* orcid.org/0000-0002-3478-0215

Osamu Yamamuro − *Institute for Solid State Physics, University of Tokyo, Kashiwa, Chiba 277-8581, Japan;* orcid.org/0000-0002-5456-8932

David L. Price − *CNRS and Université d'Orléans, CEMHTI, 45071 Orléans, France*

Complete contact information is available at: https://pubs.acs.org/10.1021/acs.jpclett.3c03145

Notes

The authors declare no competing financial interest.

■ ACKNOWLEDGMENTS

The authors thank Dr. Vitali Prakapenka for calibration of the Brillouin system at the Advanced Photon Source (APS), which made the Brillouin scattering experiments possible. Tsuyoshi Yamaguchi was supported by Grants-in-Aid for Scientific Research (KAKENHI) from the Japan Society for the Promotion of Science (JSPS) (19K03768 and 23K04665). Part of this work was performed at GeoSoilEnviroCARS (The University of Chicago, Sector 13), APS, Argonne National Laboratory. GeoSoilEnviroCARS is supported by the National Science Foundation, Division of Earth Sciences (EAR, 1634415). This research used resources of the APS, a U.S. Department of Energy (DOE) Office of Science User Facility operated for the DOE Office of Science by Argonne National Laboratory under Contract DE-AC02-06CH11357. O.B. acknowledges support from the US Army, DEVCOM Army Research Laboratory and the Joint Center for Energy Storage Research (JCESR) funded by Department of Energy through IAA SN2020957.

■ REFERENCES

(1) Suo, L.; Borodin, O.; Gao, T.; Olguin, M.; Ho, J.; Fan, X.; Luo, C.; Wang, C.; Xu, K. "Water-in-salt" electrolyte enables high-voltage aqueous lithium-ion chemistries. *Science* **2015**, *350*, 938−943.

(2) Borodin, O.; Suo, L.; Gobet, M.; Ren, X.; Wang, F.; Faraone, A.; Peng, J.; Olguin, M.; Schroeder, M.; Ding, M. S.; Gobrogge, E.; von Wald Cresce, A.; Munoz, S.; Dura, J. A.; Greenbaum, S.; Wang, C.; Xu, K. Liquid structure with nano-heterogeneity promotes cationic transport in concentrated electrolytes. *ACS Nano* **2017**, *11*, 10462−10471.

(3) González, M. A.; Akiba, H.; Borodin, O.; Cuello, G. J.; Hennet, L.; Kohara, S.; Maginn, E. J.; Mangin-Thro, L.; Yamamuro, O.; Zhang, Y.; Price, D. L.; Saboungi, M.-L. Structure of water-in-salt and water-in-bisalt electrolytes. *Phys. Chem. Chem. Phys.* **2022**, *24*, 10727−10736.

(4) Zhang, Y.; Lewis, N. H. C.; Mars, J.; Wan, G.; Weadock, N. J.; Takacs, C. J.; Lukatskaya, M. R.; Steinrück, H.-G.; Toney, M. F.; Tokmakoff, A.; Maginn, E. J. Water-in-Salt LiTFSI aqueous electrolytes. 1. Liquid structure from combined molecular dynamics simulation and experimental studies. *J. Phys. Chem. B* **2021**, *125*, 4501−4513.

(5) González, M. A.; Borodin, O.; Kofu, M.; Shibata, K.; Yamada, T.; Yamamuro, O.; Xu, K.; Price, D. L.; Saboungi, M.-L. Nanoscale relaxation in "water-in-salt" and "water-in-bisalt" electrolytes. *J. Phys. Chem. Lett.* **2020**, *11*, 7279−7284.

(6) Popov, I.; Sacci, R. L.; Sanders, N. C.; Matsumoto, R. A.; Thompson, M. W.; Osti, N. C.; Kobayashi, T.; Tyagi, M.; Mamontov, E.; Pruski, M.; Cummings, P. T.; Sokolov, A. P. Critical role of anion-solvent interactions for dynamics of solvent-in-salt solutions. *J. Phys. Chem. C* **2020**, *124*, 8457−8466.

(7) McEldrew, M.; Goodwin, Z. A. H.; Bi, S.; Kornyshev, A. A.; Bazant, M. Z. Ion clusters and networks in water-in-salt electrolytes. *J. Electrochem. Soc.* **2021**, *168*, 050514.

(8) McEldrew, M.; Goodwin, Z. A. H.; Molinari, N.; Kozinsky, B.; Kornyshev, A. A.; Bazant, M. Z. Salt-in-ionic-liquid electrolytes: Ion network formation and negative effective charges of alkali metal cations. *J. Phys. Chem. B* **2021**, *125*, 13752−13766.

(9) Angell, C. A.; Liu, C.; Sanchez, E. Rubbery solid electrolytes with dominant cationic transport and high ambient conductivity. *Nature* **1993**, *362*, 137−139.

(10) Yamaguchi, T.; Matsuoka, T. Measurement of complex shear viscosity up to 3 GHz using an electrodeless AT-cut quartz transducer. *Jpn. J. Appl. Phys.* **2022**, *61*, SG1021.

(11) Borodin, O.; Smith, G. D.; Kim, H. Viscosity of a room-temperature ionic liquid: Predictions from non-equilibrium and equilibrium molecular dynamics simulations. *J. Phys. Chem. B* **2009**, *113*, 4771−4774.

(12) Schulz, J. C. F.; Schlaich, A.; Heyden, M.; Netz, R. R.; Kappler, J. Molecular interpretation of the non-Newtonian viscoelastic behavior of liquid water at high frequencies. *Phys. Rev. Fluids* **2020**, *5*, 103301.

(13) Dukhin, A. S.; Goetz, P. J. Bulk viscosity and compressibility measurement using acoustic spectroscopy. *J. Chem. Phys.* **2009**, *130*, 124519.

(14) Lamb, H. *Hydrodynamics*, 6th ed.; Dover Publications: Mineola, NY, 1932.

(15) Holmes, M. J.; Parker, N. G.; Povey, M. J. W. Temperature dependence of bulk viscosity in water using acoustic spectroscopy. *J. Phys.: Conf. Ser.* **2011**, *269*, 012011.

(16) Jaeger, F.; Matar, O. K.; Müller, E. A. Bulk viscosity of molecular fluids. *J. Chem. Phys.* **2018**, *148*, 174504.

(17) Yamaguchi, T.; Hayakawa, M.; Matsuoka, T.; Koda, S. Electric and mechanical relaxations of $LiClO_4$−propylene carbonate systems in 100 MHz region. *J. Phys. Chem. B* **2009**, *113*, 11988−11998.

(18) Yamaguchi, T.; Mikawa, K.-i.; Koda, S. Shear relaxation of water−ionic liquid mixtures. *Bull. Chem. Soc. Jpn.* **2012**, *85*, 701−705.

(19) Sinogeikin, S.; Bass, J.; Prakapenka, V.; Lakshtanov, D.; Shen, G.; Sanchez-Valle, C.; Rivers, M. Brillouin spectrometer interfaced with synchrotron radiation for simultaneous X-ray density and acoustic velocity measurements. *Rev. Sci. Instrum.* **2006**, *77*, 103905.

(20) Ryu, Y. J.; Wang, Y.; Yu, T.; Bonnet, F.; Greenberg, E.; Prescher, C.; Prakapenka, V. B.; Tkachev, S.; Eng, P.; Stubbs, J. E.; Dera, P.; Watson, H.; Rivers, M. L. A multi-faceted experimental study on the dynamic behavior of $MgSiO_3$ glass in the Earth's deep interior. *Am. Mineral.* **2022**, *107*, 1313−1324.